Research Square

Preprints are preliminary reports that have not undergone peer review.
They should not be considered conclusive, used to inform clinical practice,
or referenced by the media as validated information.

Engineered probiotic co-expressing IL-10 and Amuc_1100 modulates the gut-brain axis to improve ASD-like behaviors in BTBR mice

Huiping Li

lihuiping@fudan.edu.cn

Children's hospital of Fudan university

Yanfeng Li
Zhengyi Liang
Yongxia Ji
Yali Lin
Xin Wang
Shu Liu
Xiangyin Xie
Yaoting Zhang
Xiubin Tong
Li Zhong

Article

Keywords:

Posted Date: October 12th, 2026

DOI: https://doi.org/10.21203/rs.3.rs-11180700/v1

License: This work is licensed under a Creative Commons Attribution 4.0 International License.
Read Full License

Additional Declarations: The authors have declared there is **NO** conflict of interest to disclose

Abstract

Autism spectrum disorder (ASD) is a neurodevelopmental disease characterized by social deficits and repetitive behaviors, yet no pharmacotherapy targeting its core symptoms currently exists. Immune dysregulation and neuroinflammation are increasingly recognized as key contributors to ASD pathogenesis, with deficient anti-inflammatory cytokine interleukin-10 (IL-10) representing a potential therapeutic target. However, systemic IL-10 delivery is limited by short half-life, poor bioavailability, and off-target toxicity. Here, we developed an engineered *Escherichia coli* Nissle 1917 strain that constitutively co-expresses murine IL-10 and the *Akkermansia muciniphila* outer membrane protein Amuc_1100 for oral delivery, and evaluated its therapeutic efficacy in the BTBR mouse model of ASD. Daily oral administration of IL-10/Amuc_1100-engineered bacteria to BTBR mice for four weeks significantly rescued sociability deficits in the three-chamber test and attenuated repetitive grooming behaviors. Mechanistically, the treatment alleviated intestinal inflammation, as evidenced by improved villus architecture and reduced lipocalin-2 levels, and remodeled the gut microbiota by increasing beneficial genera such as *Muribaculum* and *Prevotella* while suppressing pro-inflammatory taxa. In the medial prefrontal cortex (mPFC), treatment downregulated the IL-17 signaling pathway and reduced expression of pro-inflammatory genes including *Tnf* and *Il17e*. Single-cell RNA sequencing of mPFC microglia revealed a shift from a disease-associated inflammatory state toward a homeostatic, neuroprotective phenotype, accompanied by reduced pathological synaptic pruning. Collectively, these findings provide proof-of-concept evidence that oral delivery of IL-10/Amuc_1100 via an engineered probiotic is sufficient to induce concurrent changes in peripheral inflammation, central IL-17 signaling, and microglial state, together with behavioral improvements in BTBR mice. While further studies are required to establish causal relationships and long-term safety, this approach warrants consideration as a potential oral therapeutic strategy for ASD.

INTRODUCTION

Autism spectrum disorder (ASD) is a heterogeneous neurodevelopmental condition characterized by persistent deficits in social communication and interaction, as well as restricted, repetitive patterns of behavior or interests. The global prevalence of ASD has been steadily increasing; recent estimates from the US Centers for Disease Control and Prevention indicate that 1 in 31 children aged 8 years is diagnosed with ASD[1], and the known prevalence in China reaches approximately 0.7%[2]. Despite intensive research efforts, the exact etiology of ASD remains incompletely understood, and no pharmacotherapy targeting the core symptoms is currently available, highlighting an urgent need for novel therapeutic strategies.

Accumulating evidence points to immune dysregulation as a key contributor to the pathogenesis of ASD. Individuals with ASD exhibit a systemic imbalance between pro-inflammatory and anti-inflammatory responses. For instance, children with ASD show significantly elevated levels of pro-inflammatory cytokines and reduced levels of key anti-inflammatory cytokines such as interleukin-10 (IL-10)[3]. Activation of multiple inflammasome complexes leads to sustained release of IL-1β and IL-18[4], while

peripheral immune cell profiling reveals increased monocyte counts and upregulation of activation markers, as well as numerical abnormalities in various lymphocyte subsets[5]. Among helper T cell subsets, the proportion of pro-inflammatory Th17 cells is elevated, whereas regulatory T cells (Tregs) are reduced[6,7], directly disrupting immune homeostasis. Within the central nervous system (CNS), individuals with ASD display sustained microglial and monocytic activation throughout life[8]. Postmortem studies have shown increased microglial density and enhanced expression of activation markers in the brains of ASD patients[9], indicating that aberrant activation of the innate immune system is an integral component of ASD neuropathology. The origins of immune abnormalities can be traced back to early development. Maternal infection or autoimmune diseases during pregnancy significantly increase the risk of neurodevelopmental disorders, including ASD, in offspring[10,11]. Animal models of maternal immune activation have demonstrated that gestational inflammation directly induces ASD-like behaviors in progeny, accompanied by evidence of innate immune activation[12]. These findings strongly suggest that immune dysfunction is not merely an epiphenomenon of ASD but rather a key driver of neural and behavioral alterations, and that restoring immune homeostasis, particularly by replenishing deficient anti-inflammatory cytokines, holds promise as a therapeutic strategy.

IL-10 is a prototypical anti-inflammatory cytokine produced mainly by Treg cells, Breg cells, and M2 macrophages. It exerts its effects by activating STAT3 signaling, thereby suppressing antigen-presenting cell activation, downregulating MHC-II and co-stimulatory molecules, and blocking T-cell-mediated inflammatory cascades. Within the CNS, IL-10 potently inhibits microglial production of neurotoxic factors such as TNF-α and IL-6, promoting neuronal survival and synaptic plasticity[13]. Notably, the BTBR T^{+} Itpr3□□/J (BTBR) mouse strain, a well-established ASD model that recapitulates social deficits and repetitive behaviors[14], exhibits elevated basal pro-inflammatory cytokines and neuroinflammation, closely mimicking the immune phenotype of human ASD. Importantly, BTBR mice have reduced numbers of Treg cells and decreased IL-10 levels in the CNS and cervical draining lymph nodes[15]. These observations provided the rationale for our hypothesis that replenishing IL-10 might ameliorate ASD-like phenotypes.

To overcome the inherent limitations of cytokine therapy—short half-life, rapid degradation in vivo, and off-target toxicity upon systemic administration—we turned to an orally delivered engineered probiotic platform. Unlike conventional small-molecule immunomodulators that broadly suppress immune pathways or systemically administered recombinant cytokines that suffer from poor pharmacokinetics, our approach leverages a living bacterial chassis to achieve sustained, gut-restricted production of therapeutic proteins with minimal systemic exposure. The probiotic *Escherichia coli* strain Nissle 1917 (EcN) has a long history of safe use in humans, with clinical studies confirming its favorable safety profile and efficacy in maintaining remission of ulcerative colitis[16,17]. EcN is amenable to genetic manipulation and has emerged as a preferred microbial chassis for generating living therapeutics and drug delivery vehicles[18]. Using CRISPR-Cas9-mediated homologous recombination, Guo et. al. [19] constructed an engineered EcN strain (designated EcN-EB) that constitutively co-expresses murine IL-10 together with the outer membrane protein Amuc_1100 from *Akkermansia muciniphila*, a well-

characterized immunomodulatory protein[20]. This strain (CBT4088) has been constructed and characterized in a previous patent application, demonstrating stable intestinal colonization and bioactive protein secretion[19]. The use of a clinically validated, patent-protected strain with an established safety profile in humans—coupled with the non-invasive oral route and inherent suitability for chronic administration—represents a key translational advantage of our approach over traditional biologics. Amuc_1100 enhances intestinal barrier integrity, restores microbiota balance, and suppresses systemic inflammation through modulation of TLR2/4 and JAK/STAT pathways[21].

In the present study, we orally administered EcN-EB or the control strain to one-month-old BTBR mice daily for four weeks and comprehensively evaluated behavioral, histological, and molecular outcomes[22]. Our results demonstrate that IL-10/Amuc_1100 supplementation alleviated intestinal inflammation with concurrent gut microbiota remodeling[23], significantly rescued sociability deficits and reduced repetitive grooming[24], downregulated key inflammatory pathways including IL-17 signaling, and attenuated microglial activation in the mPFC. Collectively, our findings indicate that gut-delivered IL-10/Amuc_1100 can ameliorate core ASD-like behaviors and suppress both peripheral and central inflammation through modulation of the gut–brain axis[25], offering a promising new avenue for ASD treatment.

MATERIALS AND METHODS

Mice

Male BTBR T+ Itpr3□□/J (BTBR) and C57BL/6J wild-type mice were purchased from Beiyou Biology (Beijing, China). All mice were housed under specific-pathogen-free conditions with a 12-hour light/dark cycle and had ad libitum access to food and water. Mice were randomly assigned to experimental groups. Mice were randomly assigned for biological analyses, with investigators blinded to group allocation during experiments and outcome assessments. All animal procedures were approved by the Animal Care and Ethical Committee of Children's Hospital of Fudan University (no. [2026] 19) and conducted in accordance with institutional guidelines.

Bacterial strain engineering and oral gavage

The engineered Escherichia coli Nissle 1917 strain co-expressing murine IL-10 and Amuc_1100 (designated EcN EB) and the corresponding isogenic control strain were kindly provided by Hedu Biosciences Co., Ltd. The EcN EB strain (CBT4088) was previously constructed and characterized as described in Chinese Patent No. CN 118541470 A. The recombinant *Escherichia coli* Nissle 1917 strain was engineered to constitutively co-express murine interleukin-10 (IL-10) and the outer membrane protein Amuc_1100 derived from *Akkermansia muciniphila*. The isogenic control strain harbored the same expression vector without the two transgenes. Both strains were cultured overnight in Luria-Bertani (LB) broth containing appropriate antibiotics, harvested by centrifugation, washed twice with sterile

phosphate-buffered saline (PBS), and adjusted to a concentration of 1×10^9 colony-forming units (CFU) per 200 μL.

One-month-old mice were randomly divided into four groups (n = 10–11 per group): C57BL/6J receiving control bacteria (C57-Ctrl), C57BL/6J receiving engineered bacteria (C57-EB), BTBR receiving control bacteria (BTBR-Ctrl), and BTBR receiving engineered bacteria (BTBR-EB). Each mouse was orally gavaged daily with 200 μL of the respective bacterial suspension for four consecutive weeks. Behavioral tests were initiated one week after the final gavage.

Behavioral tests

All behavioral tests were conducted one week after the final gavage by investigators blinded to group assignments.

Three-chamber social interaction test. The apparatus consisted of a rectangular box (60 cm × 40 cm × 22 cm) divided into three chambers. After a 5-min habituation phase with empty wire cups, a novel mouse (Stranger 1) was placed inside a cup in one side chamber, and an identical empty cup was placed in the opposite side chamber. The test mouse was allowed to explore for 10 min; the time spent sniffing each cup was recorded. In the subsequent social novelty phase, a second unfamiliar mouse (Stranger 2) replaced the empty cup, and sniffing times were recorded for another 10 min. The time spent sniffing each cup was recorded.

Marble-burying test. Each mouse was placed individually in a standard cage (26 cm × 20 cm × 14 cm) containing 5 cm of clean bedding, on which 20 glass marbles (diameter 1.5 cm) were evenly spaced. After 20 min of free exploration, the number of marbles buried (≥ 2/3 of the marble covered by bedding) was counted.

Self-grooming test. Mice were individually placed in a clean, empty plastic cage and video-recorded for 10 min after a 5-min habituation. The total duration (seconds) and the frequency of grooming episodes (each episode defined as a bout lasting ≥ 2 s) were scored offline.

Preparation of brain samples

Mice were anesthetized with isoflurane and transcardially perfused with 50 mL of ice-cold PBS. Following perfusion, the brains were carefully extracted from the skulls. For immunofluorescence staining, the brains were fixed in 4% paraformaldehyde (PFA, Sigma-Aldrich, P6148) at 4°C overnight. After fixation, the brains were transferred to a 30% sucrose solution in PBS for cryoprotection and kept at 4°C for a minimum of 48 hours or until the tissue sank to the bottom of the container. Subsequently, the brains were embedded in Tissue-Tek® O.C.T. Compound (SAKURA, 4583) and sectioned at 15 μm thickness using a freezing microtome (Leica CM 1950) to obtain either coronal or sagittal sections. Sections were collected on adhesion slides and stored at − 80°C until use. For biochemical analysis, the

cortex and hippocampus were dissected on ice, rapidly frozen in liquid nitrogen, and stored at − 80°C. These samples were later used for protein

and RNA extraction.

H&E staining

Freshly dissected small intestinal tissues were fixed in 4% paraformaldehyde (PFA) at 4°C overnight, then cryoprotected in 30% sucrose solution at 4°C until the tissue sank. After embedding in Tissue-Tek® O.C.T. compound, the tissues were sectioned at a thickness of 15 μm using a freezing microtome (Leica CM1950). Sections were collected onto adhesion microscope slides and stored at − 80°C until staining. For hematoxylin and eosin (H&E) staining, frozen sections were first equilibrated to room temperature, then fixed in 4% PFA for 10 min and rinsed briefly with distilled water. Staining was performed according to the manufacturer's instructions for the Solarbio H&E Staining Kit (Solarbio, Beijing, China; G1120). Briefly, sections were immersed in hematoxylin solution for 5–8 min, differentiated in 0.5% hydrochloric acid-alcohol for a few seconds, and blued in running tap water for 5 min. Subsequently, sections were stained with eosin solution for 2–3 min, dehydrated through graded ethanol (70%, 80%, 95%, and 100%), cleared in xylene, and mounted with neutral balsam. Whole-slide images were acquired using an Olympus VS200 slide scanner (Olympus, Tokyo, Japan) under a 20× objective.

Immunofluorescence

Brain sections were thawed at room temperature for 30 minutes and washed three times in PBS (5 minutes each) before staining. Sections were then blocked at room temperature for 1 hour in blocking buffer (PBS with 5% normal donkey serum and 0.5% Triton X-100). Primary antibodies were diluted in blocking buffer and applied overnight at 4°C. Following primary antibody incubation, sections were washed three times with PBS (10 minutes each). Alexa-fluorophore-conjugated secondary antibodies (Alexa Fluor 488, 594, and 647, 1:500) were then incubated with the sections for 2 hours at room temperature in the dark. After three final washes with PBS, sections were counterstained with DAPI (Sigma-Aldrich, D9542, 1 mg/mL, 1:1000) for 10 minutes at room temperature. Brain sections were blocked and incubated overnight at 4°C with primary antibodies: anti-Iba1 (1:200, Wako 019-19741). Images were obtained using a Olympus FV1000MPE-B confocal microscope. For confocal imaging, 9-μm z-stack images were acquired with 1 μm thickness per slice. Quantification of images was performed using ImageJ

ELISA for Lipocalin-2 (LCN2)

Snap-frozen small intestinal tissue was homogenized in RIPA buffer (Thermo Fisher Scientific) containing protease and phosphatase inhibitors. After centrifugation (12,000 × g, 15 min, 4°C), the supernatant was collected. LCN2 concentration was measured using a mouse Lipocalin-2/NGAL ELISA

Kit (R&D Systems, MLCN20) following the manufacturer's protocol. Absorbance was read at 450 nm, and concentrations were normalized to total protein content determined by BCA assay.

RNA extraction and quantitative PCR (qPCR)

Total RNA from mPFC tissue was extracted using TRIzol reagent (Thermo Fisher Scientific). Reverse transcription was performed with a PrimeScript RT Master Mix (Takara) using 1 μg of total RNA. qPCR was conducted on a QuantStudio 6 Flex system using TB Green Premix Ex Taq II (Takara). The cycling conditions were: 95°C for 30 s, followed by 40 cycles of 95°C for 5 s and 60°C for 30 s. Relative expression was calculated using the $2^{-\Delta\Delta Ct}$ method and normalized to *β-actin*. Primers used were:

- *Il17e* (IL-25) F: 5'-ACAGGGACTTGAATCGGGCT-3',

• R: 5'-TCCAATGCAGGAGGCTGTGA-3'

- *Tnf* (TNF-α) F: 5'-CCCTCACACTCAGATCATCTTCT-3',

• R: 5'-GCTACGACGTGGGCTACAG-3'

- *β-actin* F: 5'-AGTGTGACGTTGACATCCGTA-3',

• R: 5'-GCCAGAGCAGTAATCTCCTTC-3'

Bulk RNA-sequencing

Total RNA was extracted from the medial prefrontal cortex (mPFC) of C57-Ctrl, BTBR-Ctrl, and BTBR-EB mice (n = 7–8 per group) using TRIzol reagent (Thermo Fisher Scientific). RNA integrity was assessed on an Agilent 2100 Bioanalyzer (RIN ≥ 8.0). mRNA was enriched from 1 μg of total RNA using oligo(dT) magnetic beads, then fragmented under elevated temperature. First-strand cDNA was synthesized with random hexamers, followed by second-strand synthesis. The double-stranded cDNA was end-repaired, A-tailed, ligated with Illumina adapters, size-selected (300–400 bp), and PCR-amplified. Libraries were sequenced on an Illumina NovaSeq 6000 platform with paired-end 150 bp (PE150) reads. Raw reads were trimmed and quality-filtered using fastp (v0.23.2). Clean reads were aligned to the mouse reference genome (GRCm39) using STAR (v2.7.9a). Gene-level counts were obtained with featureCounts (v2.0.1). Differential expression analysis between groups was performed using DESeq2 (v1.36.0) in R. Genes with $|\log_2$ fold change$| > 0.58$ and adjusted $P < 0.05$ were considered significantly differentially expressed. KEGG pathway enrichment was performed using clusterProfiler (v4.4.0).

Single-cell RNA sequencing (scRNA-seq)

Cortical tissues were collected from C57-Ctrl, BTBR-Ctrl, and BTBR-EB mice (n = 3 mice per group). For each group, tissues from three mice were pooled into a single sample prior to dissociation. Fresh tissue

was minced and enzymatically dissociated using a papain-based neural tissue dissociation kit (Miltenyi Biotec). The single-cell suspension was filtered through a 40-μm strainer, and dead cells were removed. Cell viability was assessed by trypan blue exclusion (> 80%). Single-cell libraries were prepared using the DNBelab C Series High-throughput Single-cell Library Set V3 (BGI Genomics) following the manufacturer's protocol. Briefly, cells were partitioned into nanoliter-scale droplets together with barcoded beads and lysis buffer. After cell lysis and mRNA capture, reverse transcription and second-strand synthesis were performed to generate double-stranded cDNA. The cDNA was amplified, and an independent oligo library was prepared for cell barcode and UMI quantification. Both cDNA and oligo libraries were circularized, amplified into DNA nanoballs (DNBs), and sequenced on a DNBSEQ platform (BGI) with paired-end 100 bp (PE100) reads. Raw sequencing data were processed using DNBC4tools (v2.1.1) to generate a gene-expression matrix. Reads were aligned to the mouse reference genome (GRCm39/mm10). Downstream analysis was performed with Seurat (v5.1.0) in R. Cells with < 200 or > 90th percentile of detected genes, or with mitochondrial read proportion > 15%, were excluded. Doublets were removed using DoubletDetection (v4.2). Data were normalized, and the top 2,000 highly variable genes were used for principal component analysis. Unsupervised clustering was performed at a resolution of 0.5. Cell types were annotated using the SCSA method. Differentially expressed genes (DEGs) within clusters or between groups were identified using the Wilcoxon rank-sum test ($\log_2$ fold change > 0.25, min.pct > 0.1, adjusted $P < 0.05$). KEGG pathway enrichment on DEGs was performed using the hypergeometric test, with FDR ≤ 0.05 considered significant.

Fecal metagenomic sequencing

Fresh fecal pellets were collected from BTBR-Ctrl and BTBR-EB mice (n = 6–8 per group) at the end of the treatment period. Microbial DNA was extracted using the QIAamp PowerFecal Pro DNA Kit (Qiagen). DNA integrity and concentration were assessed by agarose gel electrophoresis and a Qubit fluorometer. Libraries were prepared following the standard protocol of the BGI Metagenomics Library Kit. Briefly, 1 μg of genomic DNA was fragmented using a Covaris ultrasonicator to an average size of 200–400 bp. The fragmented DNA was end-repaired, A-tailed, and ligated with Illumina adapters. After size selection and PCR amplification, the libraries were circularized and sequenced on a DNBSEQ platform (BGI Genomics) with paired-end 150 bp (PE150) reads. Raw sequencing reads were filtered using SOAPnuke (v1.5.6) to remove adapters, low-quality reads (Q score < 20), and reads containing ambiguous bases. Host-derived reads were removed by alignment to the mouse reference genome using Bowtie2 (v2.3.4.1). Clean reads were assembled into contigs using MEGAHIT (v1.2.9) with a minimum contig length of 300 bp. Gene prediction on assembled contigs was performed with MetaGeneMark (v3.38), and predicted genes were clustered into a non-redundant gene catalog using CD-HIT (v4.8.1) with a 95% identity threshold. Taxonomic profiling was performed using Kraken2 (v2.1.1) against the NCBI NT database (or UHGG for human-related samples), and species abundance was estimated using Bracken (v2.6). Functional annotation was carried out by aligning predicted genes against the KEGG, eggNOG, CAZy, and CARD databases using DIAMOND (v2.0.4). Alpha diversity (Simpson index at gene level, Shannon index at genus level) and beta diversity (PCoA based on Bray-Curtis distance) were calculated using QIIME2 (v2023.5). Differentially abundant taxa between groups were identified using linear

discriminant analysis Effect Size (LEfSe, LDA score > 2, $P < 0.05$). Functional pathway enrichment was assessed using the hypergeometric test, with FDR ≤ 0.05 considered significant.

Statistical analysis

All statistical analyses were performed using GraphPad Prism 10.0. Data are presented as mean ± standard error of the mean (SEM). Normality was checked using the Shapiro-Wilk test. For comparisons among multiple groups, one-way or two-way analysis of variance (ANOVA) was used, followed by Tukey's post hoc test. For pairwise comparisons (e.g., metagenomic taxa abundance), the Wilcoxon rank-sum test was applied. P value < 0.05 was considered statistically significant. All experiments were performed with at least three biological replicates per group, and the exact sample sizes are indicated in the figure legends.

RESULT

Gut microbiota remodeling and reduced intestinal inflammation following IL-10/Amuc_1100 supplementation in BTBR mice.

To determine whether oral delivery of IL-10/Amuc_1100-engineered bacteria exerts peripheral anti-inflammatory effects, we first examined intestinal pathology. One-month-old BTBR mice and age-matched C57BL/6J wild-type controls were orally administered daily for four consecutive weeks. The treatment groups received an engineered bacterial strain co-expressing murine IL-10 and Amuc_1100, while the control groups received the isogenic bacterial strain lacking both expression cassettes. This resulted in four experimental groups: C57BL/6J + control bacteria (C57-Ctrl), C57BL/6J + engineered bacteria (C57-EB), BTBR + control bacteria (BTBR-Ctrl), and BTBR + engineered bacteria (BTBR-EB), with age-matched C57BL/6J mice serving as wild-type controls. Given the established role of the gut–brain axis in ASD, we examined intestinal pathology. Hematoxylin and eosin (HE) staining of colon sections revealed that BTBR-Ctrl mice displayed small intestinal villus architectural abnormalities, including villus blunting and disorganization, which were largely restored in BTBR-EB mice (Fig. 1A). Consistently, ELISA quantification of lipocalin-2 (LCN2), a sensitive biomarker of intestinal inflammation, showed elevated levels in the small intestine of BTBR-Ctrl mice, whereas BTBR-EB mice exhibited significantly reduced LCN2 levels, comparable to C57 controls (Fig. 1B). These data demonstrate that IL-10/Amuc_1100 treatment effectively alleviates intestinal inflammation in BTBR mice.

To comprehensively characterize the impact of IL-10/Amuc_1100-engineered bacteria on the intestinal ecosystem, we performed metagenomic sequencing on fecal samples from BTBR-Ctrl and BTBR-EB mice. Analysis of gene-level alpha diversity using the Simpson index revealed a significantly lower diversity in BTBR-EB mice compared to BTBR-Ctrl controls (Fig. 1C), suggesting a reduction in community evenness at the genetic level. In contrast, genus-level Shannon diversity showed a non-significant trend toward higher diversity in the treatment group ($p = 0.13$; Fig. 1D), indicating a potential increase in taxonomic richness and evenness at the genus level. The divergent responses between gene-level and genus-level metrics imply that the engineered bacteria intervention reshapes

microbial community structure in a multifaceted manner, possibly by suppressing certain low-abundance gene families while promoting a more balanced genus-level composition.

Stacked bar plots at the phylum, family, and genus levels revealed marked compositional changes following treatment (Fig. 1E–G). At the phylum level, BTBR-Ctrl mice were predominantly colonized by Bacteroidetes and Firmicutes, whereas BTBR-EB mice exhibited an expansion of several less abundant phyla, including Lenarviricota, Elusimicrobiota, and Uroviricota, alongside a contraction of Ignavibacteriota. These shifts suggest a global reconfiguration of the gut microbial architecture.

Quantitative comparisons (Fig. 1H–K) confirmed that BTBR-EB mice harbored a significantly lower relative abundance of Ignavibacteriota (Fig. 1H), a phylum that has been associated with pro-inflammatory states in some animal models. Conversely, the relative abundances of Lenarviricota (Fig. 1I), Elusimicrobiota (Fig. 1J), and Uroviricota (Fig. 1K) were significantly elevated in BTBR-EB mice. Notably, Elusimicrobiota contains species capable of fermenting diverse carbohydrates into short-chain fatty acids (SCFAs), which are known to reinforce intestinal barrier integrity and exert anti-inflammatory effects. The increase in Uroviricota (bacterial viruses) may reflect altered phage–host dynamics that accompany shifts in bacterial host populations.

At the genus level (Fig. 1L–O), BTBR-EB mice exhibited a significant reduction in Melioribacter (Fig. 1L), a genus that has been linked to gut inflammation and dysbiosis in certain pathological conditions. In contrast, three genera were significantly enriched in the treatment group: Endomicrobium (Fig. 1M), Muribaculum (Fig. 1N), and Prevotella (Fig. 1O). Muribaculum is a key member of the Muribaculaceae family, which is known to be enriched in healthy mice and positively correlated with intestinal health and the production of immunomodulatory metabolites. Prevotella species are versatile fermenters that can produce SCFAs and have been associated with reduced intestinal inflammation in some contexts, although their role is complex. The consistent elevation of these beneficial genera, together with the suppression of potentially harmful taxa such as Ignavibacteriota and Melioribacter, indicates a favorable remodeling of the gut microbiota toward a more homeostatic and anti-inflammatory configuration.

KEGG pathway enrichment analysis (Fig. 1P) revealed that lipopolysaccharide (LPS) biosynthesis-related pathways were predominantly enriched in BTBR-EB mice. While LPS is classically pro-inflammatory, the observed enrichment may reflect a compositional shift toward specific LPS-producing commensals whose LPS molecules possess lower endotoxic activity or immunomodulatory properties. This finding, together with the reduction in intestinal LCN2 levels (Fig. 1B) and the improvement in villus morphology (Fig. 1A), suggests that the overall microbial reconfiguration induced by IL-10/Amuc_1100 treatment leads to a net reduction in intestinal inflammation despite an increase in the potential for LPS biosynthesis.

Collectively, these metagenomic data demonstrate that IL-10/Amuc_1100 delivery profoundly restructures the gut microbiota of BTBR mice—reducing potentially deleterious phyla and genera while promoting beneficial, SCFA-producing, and anti-inflammatory associated taxa. This restructuring is functionally linked to the alleviation of intestinal inflammation observed in the same animals,

establishing a peripheral anti-inflammatory foundation that sets the stage for the subsequent behavioral and neuroimmune improvements.

Engineered IL-10/Amuc_1100 bacteria rescues sociability deficits and attenuates repetitive behaviors.

Having established that the treatment exerts peripheral anti-inflammatory effects, we next assessed whether these changes translate to behavioral improvements. A comprehensive behavioral battery was conducted post-treatment to assess core autistic-like behavioral domains. Social behavior was evaluated using the three-chamber test. As shown in Fig. 2, BTBR-Ctrl mice exhibited the expected deficit in sociability, spending comparable time sniffing an empty chamber (Object1) and a chamber containing a novel mouse (Stranger1). In contrast, BTBR mice treated with IL-10/Amuc_1100-engineered bacteria (BTBR-EB) showed a significant shift in this behavior, demonstrating a clear preference for Stranger1 over Object1 (Fig. 2A-B). These results indicate that the intervention rescued the impaired social approach behavior characteristic of the BTBR model. In the subsequent social novelty preference phase, when a second novel mouse (Stranger2) was introduced, none of the four groups exhibited a statistically significant preference for Stranger2 over the now-familiar Stranger1. A non-significant trend toward investigating the novel stranger was observed only in the C57-Ctrl and C57-EB groups (Fig. 2C). Both wild-type control groups consistently displayed normal sociability across all phases, confirming that the bacterial treatment itself did not alter baseline social behavior.

Repetitive and stereotyped behaviors were further assessed using the marble-burying and self-grooming tests. In the marble-burying test (Fig. 2D, E), BTBR-Ctrl mice buried a significantly higher number of marbles compared to both C57-Ctrl and C57-EB groups, confirming heightened compulsive-like behavior. Treatment with IL-10/Amuc_1100-engineered bacteria significantly reduced the number of marbles buried in BTBR-EB mice relative to the BTBR-Ctrl group, although the buried count remained modestly higher than that of the C57 controls, indicating a partial statistically significant attenuation of this phenotype. In the self-grooming test (Fig. 2F), BTBR-Ctrl mice exhibited significantly longer grooming duration and higher grooming frequency compared to C57-Ctrl and C57-EB groups. Remarkably, BTBR-EB mice showed a marked reduction in both parameters, reaching levels comparable to those of the wild-type control groups, indicating a near-complete rescue of repetitive self-grooming behavior.

These behavioral data demonstrate that oral IL-10/Amuc_1100 treatment, initiated after the establishment of peripheral anti-inflammatory effects, rescues sociability deficits and attenuates repetitive behaviors in BTBR mice. The robust behavioral rescue observed across multiple independent assays strengthens the association between gut-targeted immunomodulation and improved ASD-like phenotypes.

The IL-17 signaling pathway and inflammatory gene expression are downregulated in the mPFC following IL-10/Amuc_1100 treatment.

To further elucidate the molecular mechanisms underlying the observed neuroprotective effects, we performed bulk RNA-sequencing on mPFC tissue from C57-Ctrl, BTBR-Ctrl, and BTBR-EB mice. Principal

component analysis (PCA) revealed a clear separation in global transcriptional profiles among the three groups, indicating distinct gene expression patterns associated with genotype and treatment (Fig. 3A). Differential expression analysis between BTBR-Ctrl and BTBR-EB mice identified a set of significantly dysregulated genes, with key inflammatory mediators such as *Tnf* and *Il25* being downregulated, while certain other genes were upregulated in the treatment group (Fig. 3B). A heatmap of differentially expressed genes across all three groups demonstrated that BTBR-EB mice exhibited a broad downregulation of inflammation-associated genes compared to BTBR-Ctrl mice, with a distinct cluster of upregulated genes also observed (Fig. 3C).

To characterize the functional pathways affected by the treatment, we performed KEGG pathway enrichment analysis on all significantly differentially expressed genes ($|\log_2 FC| > 0.25$). This analysis revealed that IL-17 signaling was in the enriched pathways, along with other immune-related pathways such as cytokine-cytokine receptor interaction and TNF signaling (Fig. 3D). When we separately analyzed downregulated genes ($\log_2 FC < -0.25$), the IL-17 signaling pathway was emerged, alongside TNF signaling, Toll-like receptor signaling, and JAK-STAT signaling pathways, indicating a broad suppression of pro-inflammatory cascades in BTBR-EB mice (Fig. 3E). In contrast, upregulated genes ($\log_2 FC > 0.25$) were enriched in pathways related to organic hydroxy compound biosynthesis, melanin biosynthesis, and negative regulation of natural killer cell activation, suggesting a shift toward homeostatic and immunomodulatory processes (Fig. 3F).

We next validated key transcriptional changes at the protein-coding level using quantitative PCR. Consistent with the RNA-seq findings, the expression of *Il17e*, a critical component of the IL-17 signaling axis, was significantly elevated in the mPFC of BTBR-Ctrl mice compared to both C57-Ctrl and C57-EB groups. Chronic administration of IL-10/Amuc_1100-engineered bacteria markedly reduced *Il17e* expression in BTBR-EB mice (Fig. 3G). Similarly, *Tnf* expression was significantly higher in BTBR-Ctrl mice and was normalized to wild-type levels following treatment (Fig. 3H). These qPCR results corroborate the transcriptomic data and confirm that IL-10/Amuc_1100 supplementation effectively suppresses IL-17 and TNF-mediated neuroinflammatory signaling in the mPFC of BTBR mice.

Microglial reprogramming toward a homeostatic phenotype parallels the suppression of IL-17-mediated neuroinflammation in the mPFC of treated BTBR mice.

Having established that IL-10/Amuc_1100 treatment suppresses the IL-17 signaling pathway at the bulk level, we next examined whether this transcriptional remodeling is reflected in microglial function and state, we first assessed microglial activation and synaptic engulfment in the mPFC by immunofluorescence. Immunofluorescence staining for Iba1 (microglial marker), CD68 (phagocytic/lysosomal marker) and PSD95 (postsynaptic marker) revealed that BTBR-Ctrl mice exhibited increased $Iba1^+$ microglial density compared with C57-Ctrl mice, indicating microglial activation. In contrast, BTBR-EB mice displayed reduced $Iba1^+$ cell density, comparable to levels observed in C57-Ctrl and C57-EB groups (Fig. 4A). Quantitative analysis confirmed that the number of $Iba1^+$ cells was significantly elevated in BTBR-Ctrl mice and was significantly reduced after IL-10/Amuc_1100 treatment

(Fig. 4B). Co-staining for Iba1, CD68 and PSD95 further revealed that BTBR-Ctrl microglia contained more PSD95⁺ puncta within their somata, suggesting excessive engulfment of postsynaptic elements. Notably, BTBR-EB mice showed a marked decrease in the number of PSD95⁺ particles engulfed by Iba1⁺ microglia, indicating that IL-10/Amuc_1100 treatment reduces pathological microglial synapse elimination (Fig. 4C, D).

To dissect the transcriptional remodeling underlying these microglial changes, we performed single-cell RNA-sequencing (scRNA-seq) on microglia isolated from the mPFC of BTBR-Ctrl and BTBR-EB mice. Unsupervised clustering of all cells annotated major brain cell types based on canonical marker genes (Fig. 4E, F). Microglia were extracted and re-clustered, revealing four distinct subpopulations (clusters 0–3). To annotate their functional states, we scored each cluster using published gene signatures for homeostatic microglia (HM, Fig. 4G), disease-associated microglia (DAM, Fig. 4H) and interferon-responsive (IFN, Fig. 4I) states. Cluster 0 exhibited high HM scores and low DAM/IFN scores, indicating a homeostatic phenotype. In contrast, clusters 1 and 2 showed elevated DAM and IFN scores, consistent with an activated, disease-associated state, whereas cluster 3 displayed an intermediate profile. Projection of the two experimental conditions onto the UMAP revealed that BTBR-EB microglia were markedly shifted away from the DAM-enriched region and toward the homeostatic cluster 0 (Fig. 4J). Quantification of subpopulation fractions confirmed that BTBR-EB mice had a significantly increased proportion of homeostatic cluster 0 microglia and a corresponding reduction in DAM-like cluster 1 cells (Fig. 4K). Differential expression analysis between BTBR-EB and BTBR-Ctrl microglia identified robust transcriptional changes. Among the most significantly downregulated genes in BTBR-EB microglia were *Il31ra* (encoding a subunit of the IL-31 receptor involved in immune signaling), *Gpc5* (a cell surface proteoglycan implicated in neurodevelopment), *Fgfr3*, *Grin2c* (a subunit of the NMDA receptor) and *Gabrb1* (a GABA receptor subunit), suggesting a broad suppression of immune- and synapse-related transcripts. Conversely, upregulated genes included *Ptgds* (prostaglandin D2 synthase, linked to neuromodulation), *Cryab* (a small heat shock protein with neuroprotective functions) and *Klf4* (a transcription factor involved in anti-inflammatory responses) (Fig. 4L). A targeted heatmap of inflammatory-related genes showed that most pro-inflammatory transcripts, including several chemokines and complement components, were downregulated in BTBR-EB microglia, further supporting a treatment-induced shift away from an activated immune state (Fig. 4M).

Pathway enrichment analysis of genes upregulated in BTBR-EB microglia highlighted pathways associated with negative regulation of neuroinflammation and tissue repair. Specifically, negative regulation of NF-κB transcription factor activity and negative regulation of cytokine/chemokine production indicate an active suppression of pro-inflammatory signaling. The enrichment of response to reactive oxygen species suggests enhanced antioxidant capacity, whereas integrin-mediated signaling pathway and central nervous system myelination point to improved microglial support for synaptic integrity and remyelination. Collectively, these upregulated pathways reflect a protective microglial phenotype that limits immune activation while promoting repair (Fig. 4N). Conversely, genes downregulated in BTBR-EB microglia were enriched in pathways that are typically overactive in neuroinflammatory conditions, including microglial cell activation, macrophage activation and cytokine

production involved in immune response, confirming that the treatment dampens innate immune activation. Moreover, downregulation of synapse organization, Wnt signaling pathway, regulation of synapse structure or activity, GABAergic synapse and circadian rhythm suggests that the beneficial effect of IL-10/Amuc_1100 may also involve normalization of aberrant synaptic signaling and metabolic rhythms. The reduced enrichment of PPAR signaling pathway aligns with our earlier observation that PPARγ-dependent lipid droplet accumulation is restrained by treatment, linking metabolic reprogramming to the functional improvement (Fig. 4O).

Together, these data demonstrate that IL-10/Amuc_1100 treatment attenuates mPFC microglial activation and pathological synaptic pruning at the cellular level, and reprograms microglia from a DAM-dominant, pro-inflammatory transcriptional state toward a homeostatic, neuroprotective phenotype. This reprogramming is characterized by coordinated suppression of immune activation and restoration of synaptic- and myelination-related pathways, providing a mechanistic link between gut-targeted immunomodulation and improved brain function.

DISCUSSION

In this study, we demonstrate that oral administration of an engineered *Escherichia coli* Nissle 1917 strain co-expressing murine IL-10 and the *Akkermansia muciniphila* outer membrane protein Amuc_1100 significantly ameliorates core autistic-like behaviors in the BTBR mouse model of ASD. Treated BTBR mice showed improved sociability in the three-chamber test and reduced repetitive grooming, accompanied by alleviation of intestinal inflammation, remodeling of gut microbiota, attenuation of microglial activation in the mPFC, downregulation of the IL-17 signaling pathway, and a shift of microglial transcriptional state from inflammatory to homeostatic. These findings provide strong evidence that gut-targeted delivery of IL-10/Amuc_1100 via an engineered probiotic can modulate the gut-brain axis to improve ASD-related behavioral and neuropathological phenotypes.

The BTBR mouse strain is a well-established ASD model that recapitulates social deficits and repetitive behaviors, and it also exhibits immune and metabolic imbalances[14,26]. Importantly, BTBR mice have reduced numbers of IL-10-producing regulatory T cells and elevated neuroinflammation, mirroring the immune dysregulation observed in a subset of individuals with ASD[15]. Our approach directly replenishes the deficient anti-inflammatory cytokine IL-10 in a sustained, gut-restricted manner. Unlike systemic cytokine therapy, which is limited by short half-life, rapid degradation, and off-target toxicity, our engineered probiotic platform achieves local production in the intestine with minimal systemic exposure. EcN has a long history of safe use in humans, as demonstrated by clinical studies in ulcerative colitis[16,17], and is amenable to genetic manipulation using CRISPR-Cas9-based methods[20]. The addition of Amuc_1100, known to enhance intestinal barrier integrity and suppress systemic inflammation through TLR2/4 and JAK/STAT pathways, may synergize with IL-10 to further improve gut homeostasis. Thus, our strategy addresses two major limitations of current immune-based ASD interventions: lack of target specificity and poor delivery.

The therapeutic effects observed in BTBR mice are likely mediated through interconnected actions along the gut-brain axis. First, IL-10/Amuc_1100 treatment alleviated intestinal inflammation, as evidenced by improved villus architecture and reduced LCN2 levels. This is consistent with the established role of IL-10 in maintaining intestinal immune homeostasis and of Amuc_1100 in strengthening the gut epithelial barrier. Second, the treatment remodeled the gut microbiota, increasing the relative abundance of beneficial genera such as *Muribaculum*, *Prevotella*, and *Ligilactobacillus murinus*, while reducing pro-inflammatory taxa. *Muribaculum* has been associated with healthy gut function and immunomodulation, and *Prevotella* species are known to produce short-chain fatty acids that can influence systemic and central inflammation. These microbial changes may reduce endotoxemia and modulate peripheral immune cells that signal to the brain. Third, we observed a marked downregulation of the IL-17 signaling pathway in the mPFC, a key region for socio-emotional regulation. IL-17, particularly IL-17A, has been causally linked to ASD-like behaviors in maternal immune activation models[12], and elevated IL-17 levels have been reported in ASD patients[7]. IL-10 is known to suppress Th17 differentiation and IL-17 production via its action on regulatory T cells, and our data suggest that gut-delivered IL-10 restores the Treg/Th17 balance, thereby reducing IL-17-mediated neuroinflammation. This interpretation is supported by our bulk RNA-seq findings showing significant downregulation of IL-17 pathway genes and by qPCR validation of decreased *Il17e* and *Tnf* expression. While Lee et al. focused on neuronal IL-17 receptor expression, our transcriptomic analysis reveals that IL-17-associated pathways are also modulated in microglia upon gut-targeted immunomodulation. This suggests that the cortical IL-17 system may involve both direct neuronal and glial components, with microglia potentially serving as both sensors and amplifiers of IL-17-mediated neuroimmune signaling.

A critical mechanistic insight comes from our single-cell RNA-sequencing analysis of cortical microglia. We found that IL-10/Amuc_1100 treatment shifted microglial identity from an inflammatory state (characterized by high expression of *Il1b*, *Tnf*, and *Ccl2*) toward a homeostatic state (characterized by *P2ry12*, *Tmem119*, and *Cx3cr1*). Pathway enrichment analysis revealed that downregulated genes in inflammatory microglia were enriched in pro-inflammatory cascades such as positive regulation of cell adhesion and WNT signaling, both of which have been implicated in aberrant synaptic connectivity and neuroinflammation in ASD. Conversely, upregulated genes were enriched in negative regulation of cytokine production and immune response. Moreover, we directly detected activation of IL-10 downstream target genes in BTBR-EB microglia, providing evidence that the orally administered probiotic engages IL-10 signaling within the brain. This microglial reprogramming likely underlies the observed reduction in microglial density and the overall attenuation of neuroinflammation, ultimately contributing to the improvement in social behavior and reduction in repetitive behaviors.

When considered in the broader context of immune-based interventions for ASD, our approach is mechanistically and practically distinct from existing strategies. Broad-spectrum anti-inflammatory drugs—such as corticosteroids, minocycline, and celecoxib—have been tested in ASD with inconsistent efficacy and do not address the specific IL-10 deficit that characterizes a subset of patients. Low-dose IL-2, which expands regulatory T cells, has shown some benefit but carries risks of systemic immune

activation and requires parenteral administration[27]. More recently, pharmacological targeting of specific immune pathways—including Th17/RORγt signaling via adenosine A2A receptor activation[28], CCR5 antagonism, and histamine H4 receptor blockade—has been explored in preclinical ASD models[29,30], but these approaches rely on systemic delivery of small-molecule inhibitors that directly suppress individual pro-inflammatory cascades. Our strategy is conceptually and mechanistically distinct from all of these: rather than systemically inhibiting a single inflammatory pathway, we orally deliver a living bacterial platform that restores the physiological balance of the anti-inflammatory cytokine IL-10 at the intestinal mucosa, thereby coordinating a multi-tiered immunomodulatory response engaging the gut, the microbiota, and the brain. This gut-restricted, self-sustaining delivery system leverages the body's own regulatory mechanisms rather than imposing exogenous pharmacological blockade, and it is inherently non-invasive and suitable for chronic administration. Importantly, the translational potential of this approach is supported by clinical validation of the EcN chassis itself: an oral EcN strain expressing IL-10 and autoantigens has been well tolerated in a Phase 2a study in type 1 diabetes, and EcN has an established safety record in humans from ulcerative colitis trials[31]. These comparisons underscore that our strategy is not only mechanistically novel but also practically positioned for eventual clinical translation.

Several limitations of this study should be acknowledged. First, we used only the BTBR model, which represents an immune-driven subtype of ASD. Whether similar efficacy is observed in other ASD models, such as Mecp2 KO or maternal immune activation (MIA) mice, remains to be tested. Second, the relative contribution of IL-10 versus Amuc_1100 to the overall therapeutic effect was not dissected. While both molecules have independent anti-inflammatory and barrier-enhancing properties, future studies using single-expression constructs (IL-10 only or Amuc_1100 only) are needed to determine potential synergy. Third, we did not perform long-term safety or toxicology assessments beyond the four-week treatment period. Although EcN has an established safety record[16,17], chronic exposure to engineered bacteria secreting immunomodulatory proteins warrants careful evaluation, including assessment of anti-drug antibody formation and potential off-target effects. Fourth, the precise molecular route by which gut-delivered IL-10 influences brain microglia remained to be fully elucidated. Possibilities include direct entry of small amounts of IL-10 or its downstream mediators into the circulation and across the blood-brain barrier, modulation of gut-derived metabolites that affect CNS immune cells, or vagal nerve signaling. Our observation that IL-10 downstream targets are upregulated in microglia suggests functional engagement of the IL-10 pathway in the brain, but the exact signaling cascade requires further investigation.

In conclusion, this study provides proof-of-concept that an orally delivered engineered probiotic co-expressing IL-10 and Amuc_1100 can ameliorate core ASD-like behaviors in BTBR mice through coordinated anti-inflammatory actions on the gut, microbiota, and brain, including suppression of the IL-17 signaling pathway and reprogramming of microglia from a pro-inflammatory to a homeostatic state. Given the favorable safety profile of EcN in humans and the non-invasive oral route, this approach holds

promise for clinical translation as a disease-modifying therapy for ASD, a condition with no currently approved pharmacotherapy for its core symptoms.

Declarations

Conflict of Interest

The authors declare no conflict of interest.

Acknowledgements

We thank Dr. Bin Xiang of Hedu Biosciences Co., Ltd. for providing the engineered bacterial strains used in this study. We thank Dr. Min Zhang and Dr. Yi Lu from Xiamen Children's Hospital for their valuable support and assistance with this study. This study was supported by grants from the Xiamen Key Healthcare Projects (3502Z20234020 to H.L.), the Natural Science Foundation of Fujian Province (2025D007 to H.L.), the Innovative Drug Research and Development–National Science and Technology Major Project (2026ZD1807700 and 2026ZD1807701 to L.Z.); the National Natural Science Foundation of China (82522029 and 32471045 to L.Z.); the Guangdong Basic and Applied Basic Research Foundation (2025A1515011305 to L.Z.); the Fundamental Research Funds for the Chinese Central Universities (20720250184 to L.Z.).

References

1. Shaw, K. A. *et al.* Prevalence and Early Identification of Autism Spectrum Disorder Among Children Aged 4 and 8 Years - Autism and Developmental Disabilities Monitoring Network, 16 Sites, United States, 2022. *MMWR Surveill Summ* 74, 1–22 (2025). https://doi.org/10.15585/mmwr.ss7402a1
2. Jiang, X., Chen, X., Su, J. & Liu, N. Prevalence of autism spectrum disorder in mainland china over the past 6 years: a systematic review and meta-analysis. *BMC Psychiatry* 24, 404 (2024). https://doi.org/10.1186/s12888-024-05729-9
3. Bryn, V. *et al.* Cytokine Profile in Autism Spectrum Disorders in Children. *J Mol Neurosci* 61, 1–7 (2017). https://doi.org/10.1007/s12031-016-0847-z
4. Saresella, M. *et al.* Multiple inflammasome complexes are activated in autistic spectrum disorders. *Brain Behav Immun* 57, 125–133 (2016). https://doi.org/10.1016/j.bbi.2016.03.009
5. Ahmad, S. F. *et al.* Upregulation of interleukin (IL)-31, a cytokine producing CXCR1 peripheral immune cells, contributes to the immune abnormalities of autism spectrum disorder. *J Neuroimmunol* 349, 577430 (2020). https://doi.org/10.1016/j.jneuroim.2020.577430
6. Moaaz, M., Youssry, S., Elfatatry, A. & El Rahman, M. A. Th17/Treg cells imbalance and their related cytokines (IL-17, IL-10 and TGF-β) in children with autism spectrum disorder. *J Neuroimmunol* 337, 577071 (2019). https://doi.org/10.1016/j.jneuroim.2019.577071

7. Nadeem, A. *et al.* Oxidative and inflammatory mediators are upregulated in neutrophils of autistic children: Role of IL-17A receptor signaling. *Prog Neuropsychopharmacol Biol Psychiatry* 90, 204–211 (2019). https://doi.org/10.1016/j.pnpbp.2018.12.002
8. Morgan, J. T. *et al.* Microglial activation and increased microglial density observed in the dorsolateral prefrontal cortex in autism. *Biol Psychiatry* 68, 368–376 (2010). https://doi.org/10.1016/j.biopsych.2010.05.024
9. Ahmad, S. F. *et al.* Involvement of CD45 cells in the development of autism spectrum disorder through dysregulation of granulocyte-macrophage colony-stimulating factor, key inflammatory cytokines, and transcription factors. *Int Immunopharmacol* 83, 106466 (2020). https://doi.org/10.1016/j.intimp.2020.106466
10. Chen, S. W. *et al.* Maternal autoimmune diseases and the risk of autism spectrum disorders in offspring: A systematic review and meta-analysis. *Behav Brain Res* 296, 61–69 (2016). https://doi.org/10.1016/j.bbr.2015.08.035
11. Brynge, M. *et al.* Maternal infection during pregnancy and likelihood of autism and intellectual disability in children in Sweden: a negative control and sibling comparison cohort study. *Lancet Psychiatry* 9, 782–791 (2022). https://doi.org/10.1016/s2215-0366(22)00264-4
12. Choi, G. B. *et al.* The maternal interleukin-17a pathway in mice promotes autism-like phenotypes in offspring. *Science* 351, 933–939 (2016). https://doi.org/10.1126/science.aad0314
13. Bido, S. *et al.* Microglia-specific IL-10 gene delivery inhibits neuroinflammation and neurodegeneration in a mouse model of Parkinson's disease. *Sci Transl Med* 16, eadm8563 (2024). https://doi.org/10.1126/scitranslmed.adm8563
14. McFarlane, H. G. *et al.* Autism-like behavioral phenotypes in BTBR T + tf/J mice. *Genes Brain Behav* 7, 152–163 (2008). https://doi.org/10.1111/j.1601-183X.2007.00330.x
15. Uddin, M. N., Manley, K. & Lawrence, D. A. Altered meningeal immunity contributing to the autism-like behavior of BTBR T (+) Itpr3 (tf) /J mice. *Brain Behav Immun Health* 26, 100563 (2022). https://doi.org/10.1016/j.bbih.2022.100563
16. Kruis, W. *et al.* Double-blind comparison of an oral Escherichia coli preparation and mesalazine in maintaining remission of ulcerative colitis. *Aliment Pharmacol Ther* 11, 853–858 (1997). https://doi.org/10.1046/j.1365-2036.1997.00225.x
17. Sonnenborn, U. & Schulze, J. The non-pathogenic Escherichia coli strain Nissle 1917 – features of a versatile probiotic. *Microbial Ecology in Health and Disease* 21, 122–158 (2009). https://doi.org/10.3109/08910600903444267
18. Yu, M., Hu, S., Tang, B., Yang, H. & Sun, D. Engineering Escherichia coli Nissle 1917 as a microbial chassis for therapeutic and industrial applications. *Biotechnol Adv* 67, 108202 (2023). https://doi.org/10.1016/j.biotechadv.2023.108202
19. Yu Qi Guo, G. X. Y., Bin Xiang. A genetically modified microorganism and its application. China patent (2024).

20. Liu, Q. *et al.* A Minimal and Portable CRISPR Platform Based on Bifidobacterial Cas9 Enables Genome Editing in E. coli Nissle 1917. *ACS Synth Biol* 15, 1544–1556 (2026). https://doi.org/10.1021/acssynbio.5c00911
21. Wu, X., Yu, D., Ma, Y., Fang, X. & Sun, P. Function and therapeutic potential of Amuc_1100, an outer membrane protein of Akkermansia muciniphila: A review. *Int J Biol Macromol* 308, 142442 (2025). https://doi.org/10.1016/j.ijbiomac.2025.142442
22. Pochakom, A. *et al.* Selective Probiotic Treatment Positively Modulates the Microbiota-Gut-Brain Axis in the BTBR Mouse Model of Autism. *Brain Sci* 12 (2022). https://doi.org/10.3390/brainsci12060781
23. Wu, X., Yu, D., Ma, Y., Fang, X. & Sun, P. Function and therapeutic potential of Amuc_1100, an outer membrane protein of Akkermansia muciniphila: A review. *International Journal of Biological Macromolecules* 308, 142442 (2025). https://doi.org/https://doi.org/10.1016/j.ijbiomac.2025.142442
24. Nettleton, J. E. *et al.* Prebiotic, Probiotic, and Synbiotic Consumption Alter Behavioral Variables and Intestinal Permeability and Microbiota in BTBR Mice. *Microorganisms* 9, 1833 (2021).
25. Feng, J. *et al.* Akkermansia muciniphila in neurological disorders: mechanisms and therapeutic potential via the gut-brain axis. *Frontiers in Neuroscience* Volume 19–2025 (2025). https://doi.org/10.3389/fnins.2025.1650807
26. Viscomi, M. P., Czyrska, J., Winiarczyk, D., Ziętek, M. M. & Sampino, S. The BTBR T+ Itpr3tf/J mouse strain as a model to study the genetic, immune, and metabolic origins of neurodevelopmental disorders. *Research in Autism Spectrum Disorders* 119, 102526 (2025). https://doi.org/https://doi.org/10.1016/j.rasd.2024.102526
27. Li, M. *et al.* LdIL-2 treatment in ASD: a novel immunotherapeutic approach targeting Th/Treg dysfunction and neuroinflammation. *Translational Psychiatry* 15, 376 (2025). https://doi.org/10.1038/s41398-025-03609-8
28. Ansari, M. A. *et al.* Adenosine A2A receptor modulates neuroimmune function through Th17/retinoid-related orphan receptor gamma t (RORγt) signaling in a BTBR T+ Itpr3tf/J mouse model of autism. *Cellular Signalling* 36, 14–24 (2017). https://doi.org/https://doi.org/10.1016/j.cellsig.2017.04.014
29. Ahmad, S. F. *et al.* DAPTA, a C-C chemokine receptor 5 (CCR5) antagonist attenuates immune aberrations by downregulating Th9/Th17 immune responses in BTBR T+ Itpr3tf/J mice. *European Journal of Pharmacology* 846, 100–108 (2019). https://doi.org/https://doi.org/10.1016/j.ejphar.2019.01.016
30. Ahmad, S. F. *et al.* The histamine-4 receptor antagonist JNJ7777120 prevents immune abnormalities by inhibiting RORγt/T-bet transcription factor signaling pathways in BTBR T+ Itpr3tf/J mice exposed to gamma rays. *Molecular Immunology* 114, 561–570 (2019). https://doi.org/https://doi.org/10.1016/j.molimm.2019.09.007

31. Sturm, A. *et al.* Escherichia coli Nissle 1917 distinctively modulates T-cell cycling and expansion via toll-like receptor 2 signaling. *Infect Immun* 73, 1452–1465 (2005). https://doi.org/10.1128/iai.73.3.1452-1465.2005

Figures

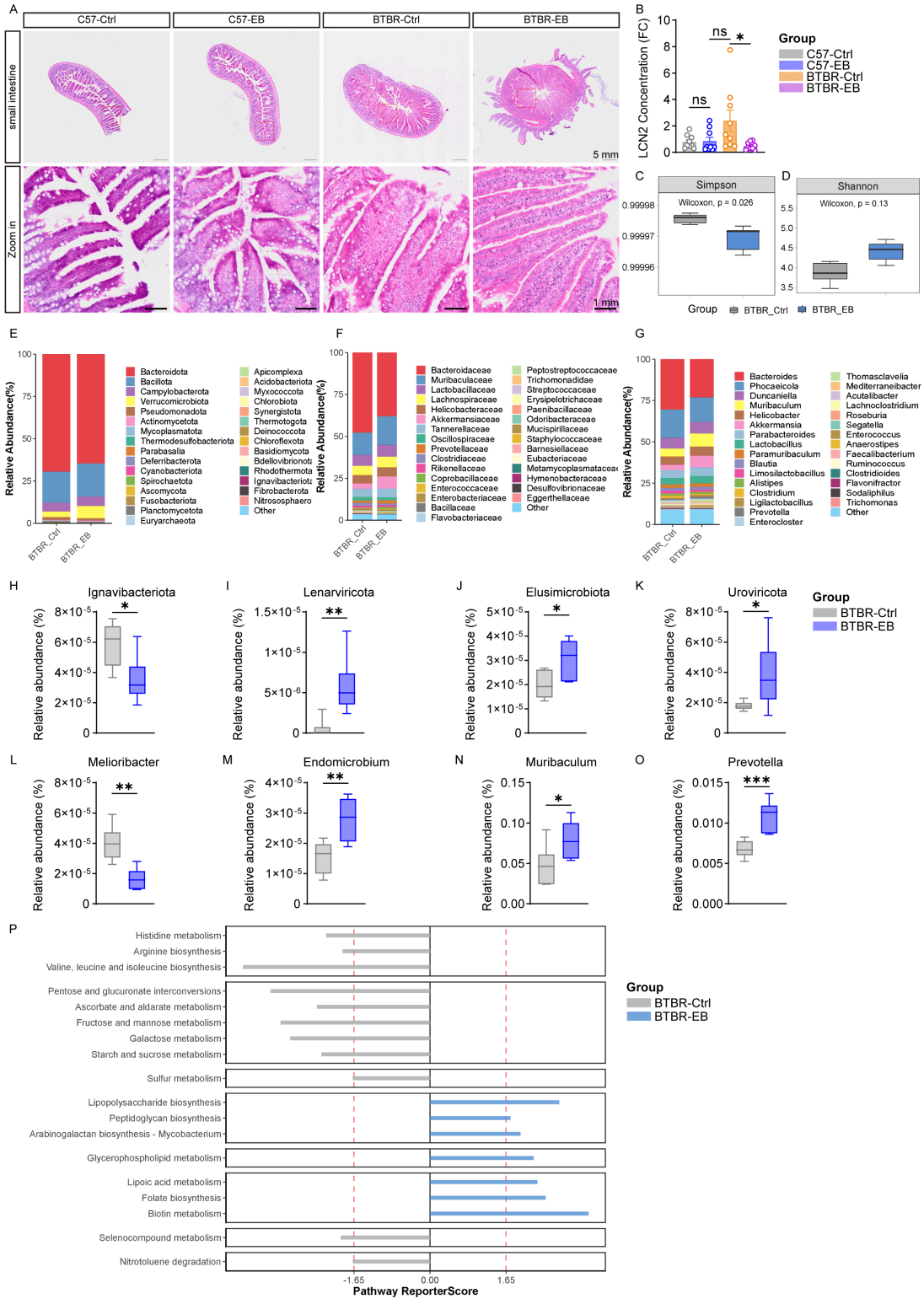


Figure 1

Metagenomic profiling reveals that IL-10/Amuc_1100-engineered bacteria reshape gut microbial diversity, taxonomic composition, and functional potential in BTBR mice. (A) HE staining of colon sections showing small intestinal villus morphology. BTBR-Ctrl mice display villus blunting and disorganization, which are ameliorated in BTBR-EB mice. Scale bar, 5 mm and 1 mm for zoom in. **(B)** ELISA quantification of LCN2 levels in small intestine homogenates. BTBR-Ctrl mice show elevated LCN2, indicating intestinal inflammation, whereas BTBR-EB mice have LCN2 levels comparable to C57 controls. Data are mean ± SEM; n = 9 mice per group. **(C)** Gene-level alpha diversity measured by the Simpson index. BTBR-EB mice show significantly lower diversity compared to BTBR-Ctrl mice (Wilcoxon test, $P < 0.05$). **(D)** Genus-level alpha diversity measured by the Shannon index. BTBR-EB mice show a non-significant trend toward higher diversity (Wilcoxon test, $P = 0.13$). **(E)** Stacked bar plot of microbial composition at the phylum level for each individual mouse. **(F)** Stacked bar plot at the family level. **(G)** Stacked bar plot at the genus level. **(H)** Relative abundance of the phylum *Ignavibacteriota* – significantly reduced in BTBR-EB mice. **(I)** Relative abundance of the phylum *Lenarviricota* – significantly increased in BTBR-EB mice. **(J)** Relative abundance of the phylum *Elusimicrobiota* – significantly increased in BTBR-EB mice. **(K)** Relative abundance of the phylum *Uroviricota* – significantly increased in BTBR-EB mice. **(L)** Relative abundance of the genus *Melioribacter* – significantly reduced in BTBR-EB mice. **(M)** Relative abundance of the genus *Endomicrobium* – significantly increased in BTBR-EB mice. **(N)** Relative abundance of the genus *Muribaculum* – significantly increased in BTBR-EB mice. **(O)** Relative abundance of the genus *Prevotella* – significantly increased in BTBR-EB mice. **(P)** KEGG enrichment analysis comparing BTBR-EB vs. BTBR-Ctrl. Pathways related to LPS biosynthesis are predominantly enriched in BTBR-EB mice (dot size: gene count; color: adjusted *P* value). For all box plots (H–O), data are presented as mean ± SEM; statistical significance was determined by Wilcoxon rank-sum test. *$P < 0.05$, **$P < 0.01$, ****$P < 0.001$.

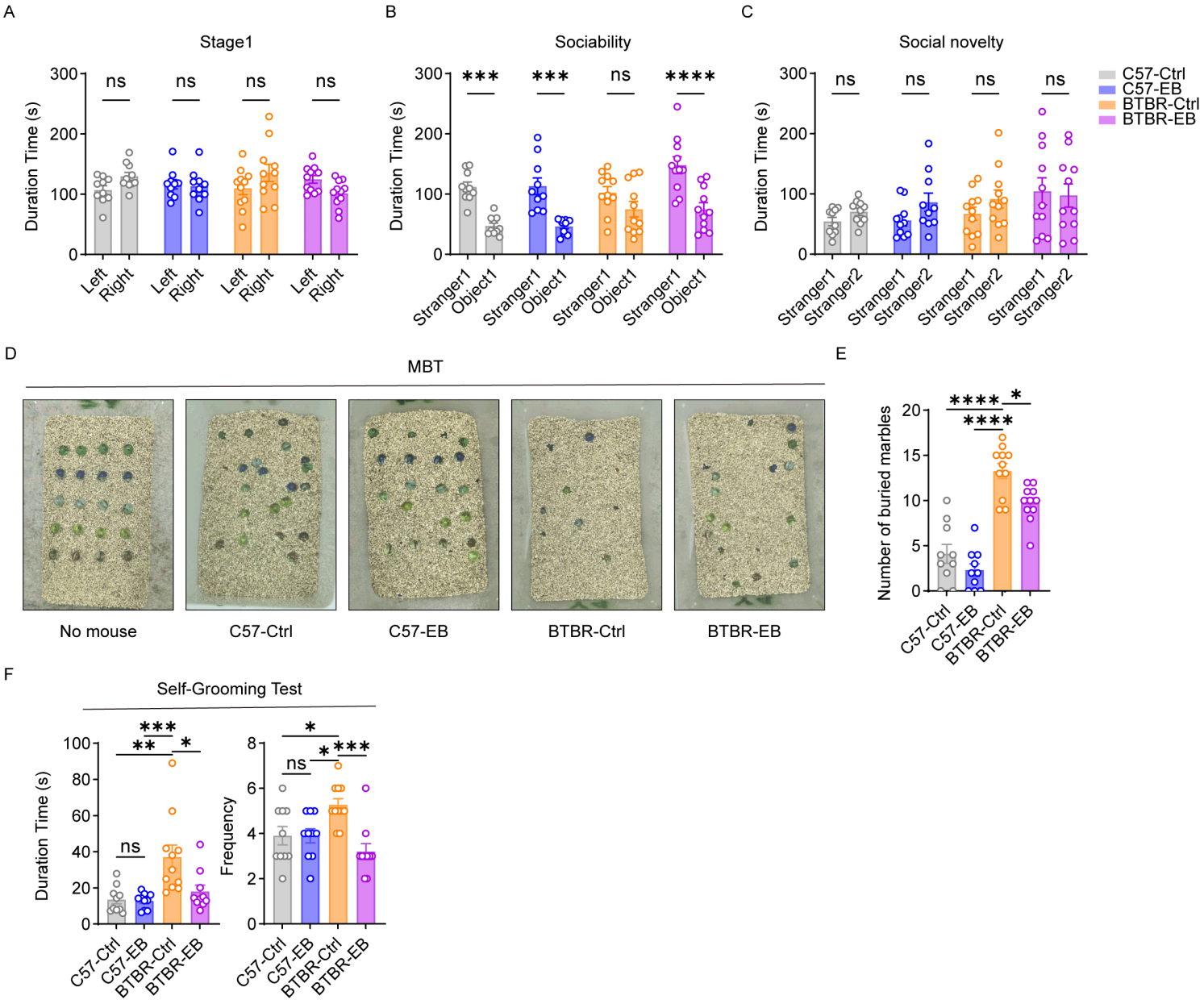


Figure 2

Oral delivery of IL-10/Amuc_1100-engineered bacteria rescues social deficits and attenuates repetitive behaviors in BTBR mice. (A-C) Three-chamber test. **(A)**Habituation phase (Stage 1): All groups showed no inherent side preference for the two empty chambers (Left and Right). **(B)** Sociability phase (Stage 2): Quantification of sniffing time directed toward an empty chamber (Object1) versus a chamber containing a novel mouse (Stranger1). BTBR-Ctrl mice showed no significant preference, whereas BTBR-EB mice spent significantly more time sniffing Stranger1 than Object1, indicating restored social approach. Data are presented as mean ± SEM; statistical analysis was performed by two-way ANOVA followed by Tukey's post hoc test (n = 10–11 mice per group). **(C)** Social novelty preference phase (Stage 3): None of the groups showed a significant preference for sniffing a novel mouse (Stranger2) over the now-familiar mouse (Stranger1). **(D)** Representative images from the marble-burying test. **(E)**Quantification of marbles buried. BTBR-Ctrl mice buried significantly more marbles than both C57-Ctrl and C57-EB groups.

BTBR-EB mice buried significantly fewer marbles than BTBR-Ctrl mice, although still slightly more than C57 controls. **(F)** Self-grooming test quantification. Left: Total grooming duration. Right: Grooming episode frequency. BTBR-Ctrl mice showed significantly increased duration and frequency compared to C57 controls. BTBR-EB mice exhibited a significant reduction in both parameters, reaching levels comparable to C57 groups. All data are presented as mean ± SEM. Statistical significance was determined by one-way ANOVA followed by Tukey's post hoc test. ns, not significant; *$P < 0.05$; **$P < 0.01$; ****$P < 0.001$.

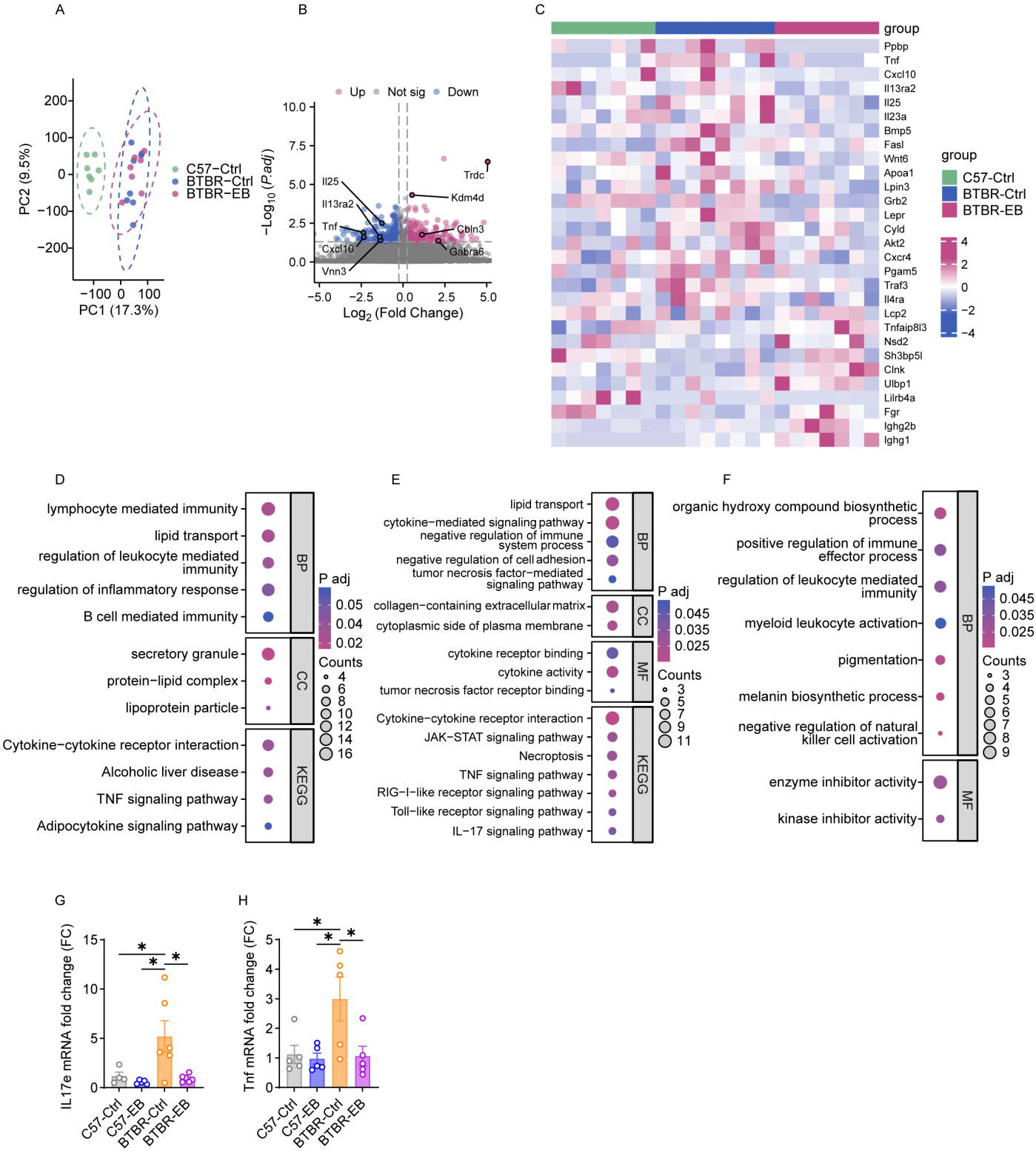


Figure 3

Transcriptomic profiling reveals suppression of IL-17 signaling and inflammatory networks, with qPCR validation. (A) Principal component analysis (PCA) plot of bulk RNA-sequencing data from mPFC tissue of C57-Ctrl, BTBR-Ctrl, and BTBR-EB mice, showing a clear separation in global gene expression profiles. **(B)**Volcano plot displaying differentially expressed genes (DEGs) between BTBR-Ctrl and BTBR-EB groups. Significantly upregulated (red) and downregulated (blue) genes are highlighted ($|\log_2 FC| > 0.25$, adjusted $P < 0.05$). Key genes such as *Trdc* (upregulated) and *Tnf*, *Il25*(downregulated) are labeled. **(C)** Heatmap of DEGs across C57-Ctrl, BTBR-Ctrl, and BTBR-EB groups. A broad downregulation of inflammation-associated genes is observed in BTBR-EB mice compared to BTBR-Ctrl, with a distinct cluster of upregulated genes also shown. **(D)**KEGG pathway enrichment analysis of all significant DEGs ($|\log_2 FC| > 0.25$) between BTBR-Ctrl and BTBR-EB. The IL-17 signaling pathway is among the top enriched pathways. Dot size represents gene count; color indicates the adjusted *P* value. **(E)** KEGG pathway enrichment analysis of significantly downregulated genes ($\log_2 FC < -0.25$) in BTBR-EB mice compared to BTBR-Ctrl. The IL-17 signaling pathway, along with TNF, Toll-like receptor, and JAK-STAT signaling pathways, is prominently downregulated. **(F)** KEGG pathway enrichment analysis of significantly upregulated genes ($\log_2 FC > 0.25$) in BTBR-EB mice compared to BTBR-Ctrl. Enriched pathways include organic hydroxy compound biosynthesis, melanin biosynthesis, and negative regulation of natural killer cell activation. **(G)** Quantitative PCR (qPCR) validation of *Il17e*expression in the mPFC. *Il17e* mRNA levels are significantly elevated in BTBR-Ctrl mice compared to both C57-Ctrl and C57-EB groups, and significantly reduced in BTBR-EB mice. **(H)** qPCR validation of *Tnf* expression in the mPFC. *Tnf* levels follow a similar pattern, with marked elevation in BTBR-Ctrl mice and restoration to wild-type levels following IL-10/Amuc_1100 treatment. All data are presented as mean ± SEM. Statistical analysis for (G) and (H) was performed by one-way ANOVA followed by Tukey's post hoc test. **P* < 0.05, ***P* < 0.01, *****P*< 0.001; ns, not significant.

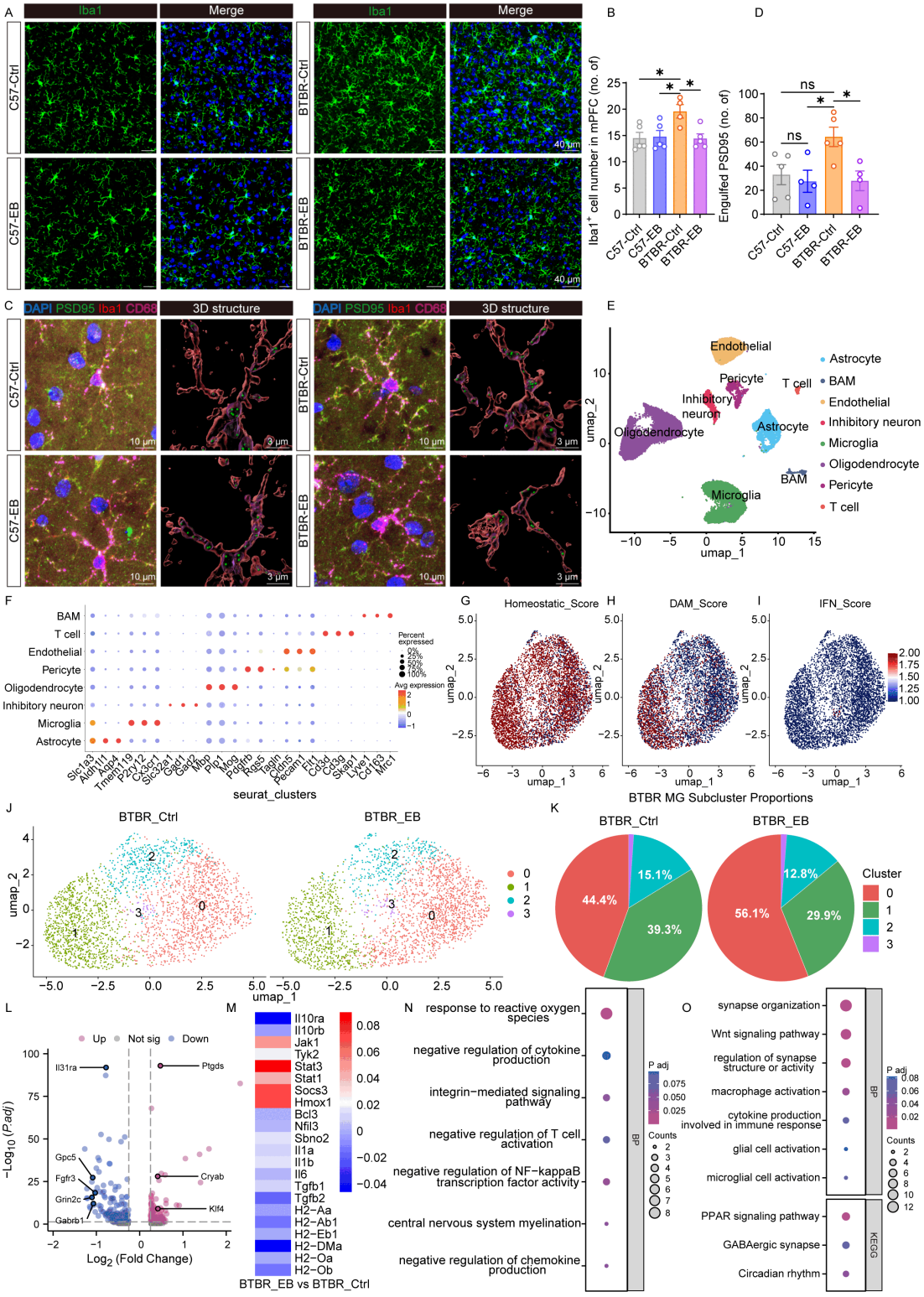


Figure 4

IL-10/Amuc_1100 treatment reduces mPFC microglial activation and pathological synaptic pruning. **(A)** Representative immunofluorescence images of Iba1 (microglia, green) and DAPI (blue) in the mPFC of C57-Ctrl, C57-EB, BTBR-Ctrl and BTBR-EB mice. Scale bar, 40 μm. **(B)** Quantification of Iba1$^+$ cell density in the mPFC. BTBR-Ctrl mice show a significant increase in microglial number, which is reversed by IL-10/Amuc_1100 treatment. Data are mean ± SEM; n = 4–5 mice per group. **(C)** Representative

images of Iba1 (red), CD68 (purple), PSD95 (green) and DAPI (blue) co-staining in the mPFC. Scale bar, 10 μm, and 3 μm for 3D structure. **(D)** Quantification of PSD95 puncta engulfed by $Iba1^+$ microglia per cell. BTBR-EB mice exhibit a significant reduction in microglial PSD95 engulfment compared with BTBR-Ctrl mice. Data are mean ± SEM; n = 4–5 mice per group. Statistical analyses were performed using one-way ANOVA with Tukey's multiple-comparisons test (B, D). **(E)** UMAP visualization of all major cell types identified from mPFC single-cell RNA-seq of BTBR-Ctrl and BTBR-EB mice, colored by cell type annotation. **(F)** Dot plot showing the expression of canonical marker genes used to define each major cell type. Dot size represents the percentage of cells expressing the gene, and color intensity indicates average expression level. **(G–I),** Signature scoring of microglial subpopulations for homeostatic microglia (HM) (**G**), disease-associated microglia (DAM) (**H**) and interferon-responsive (IFN) (**I**) gene signatures. Cluster 0 exhibits high HM scores and low DAM/IFN scores, whereas clusters 1 and 2 show elevated DAM and IFN scores. **(J)** UMAP projections of microglia split by experimental group (BTBR-Ctrl vs. BTBR-EB), highlighting the shift toward homeostatic cluster 0 in BTBR-EB mice. **(K)** Stacked bar plot showing the relative proportions of each microglial subpopulation in BTBR-Ctrl and BTBR-EB mice. BTBR-EB mice show a significant increase in homeostatic cluster 0 and a decrease in DAM-like cluster 1. **(L)** Volcano plot of differentially expressed genes in BTBR-EB versus BTBR-Ctrl microglia. Significantly downregulated genes and upregulated genes are highlighted. **(M)** Heatmap showing $\log_2$ fold-change (BTBR-EB vs. BTBR-Ctrl) of selected inflammatory-related genes, demonstrating broad downregulation of pro-inflammatory transcripts after treatment. **(N)** Dot plot of GO and KEGG pathway enrichment analysis for genes significantly upregulated in BTBR-EB microglia. Enriched pathways include response to reactive oxygen species, negative regulation of cytokine production, integrin-mediated signaling pathway, regulation of T cell activation, negative regulation of NF-κB transcription factor activity, central nervous system myelination and negative regulation of chemokine production. **(O)** Dot plot of GO and KEGG pathway enrichment analysis for genes significantly downregulated in BTBR-EB microglia. Downregulated pathways include synapse organization, Wnt signaling pathway, regulation of synapse structure or activity, macrophage activation, cytokine production involved in immune response, glial cell activation, microglial cell activation, PPAR signaling pathway, GABAergic synapse and circadian rhythm. Data are representative of three independent experiments with n = 3 mice per group. For differential expression, genes with $|\log_2 FC| > 0.25$ and adjusted $P < 0.05$ were considered significant. Statistical details are provided in the Methods. All data are presented as mean ± SEM. Statistical analysis for (B) and (D) was performed by one-way ANOVA followed by Tukey's post hoc test. *$P < 0.05$, **$P < 0.01$, ****$P < 0.001$; ns, not significant.